AUT Journal of Modeling and Simulation

AUT J. Model. Simul., 49(1)(2017)103-112
DOI: 10.22060/miscj.2016.834

Adaptive Control of a Spin-Stabilized Spacecraft Using two Reaction Wheels and a 1DoF Gimbaled-Thruster

H. Kouhi[1], M. Kabganian[1*], F. Fani Saberi[2], M. Shahravi[3]

[1] Department of Mechanical Engineering, Amirkabir University of Technology, Tehran, Iran
[2] Space Science and Technology Institute, Amirkabir University of Technology, Tehran, Iran
[3] Space Research Institute, Tehran, Iran

ABSTRACT: In impulsive orbital maneuvers, a large disturbance torque is generated by the thrust vector misalignment from the center of mass (C.M). The purpose of this paper is to reject the mentioned disturbance and stabilize the spacecraft attitude, based on the combination of a one degree of freedom (1DoF) gimbaled-thruster, two reaction wheels (RWs) and spin-stabilization. In this paper, the disturbances are assumed to be unknown and reaction control systems (RCS) are not employed. The nonlinear two-body dynamics of the proposed system is formulated and validated by the Simmechanics model. The closed-loop controller includes a full state feedback controller based on the gimbal actuator, a self-tuning controller (STC) based on the two RWs and a least squares based disturbance estimator. The simulation results are given by which the applicability of the proposed method is illustrated.

Review History:

Received: 5 March 2016
Revised: 30 September 2016
Accepted: 18 October 2016
Available Online: 23 October 2016

Keywords:

Impulsive thrusting Maneuver
Gimbaled-Thruster
Spin-Stabilization
Reaction Wheel
Thrust Vector Misalignment
Disturbance Estimator
Self-Tuning Controller

1- Introduction

In an impulsive orbital maneuver a large thrust force in a short time is used to generate a velocity increment Δv. Thrust vector offset from the C.M, always exists (see [1]) that generates a large disturbance torque, by which the attitude instability may be occurred; it is clear that it results in a thrust vector deviation from the desired inertial direction. As a result, a high capacity attitude control system is needed to compensate the mentioned large exogenous disturbances.

The attitude control systems for thrusting maneuver are classified as: 1) spin-stabilization 2) based on RCSs, and 3) a combination of a RCS and thrust vector control (TVC) (see [2]), and 4) the combination of TVC scheme and spin-stabilization ([3]).

Spin-stabilization as a simple and low cost method, is used in orbital maneuvers of small satellites and spacecraft [4, 5]. The thrusters used for spin and despin are simpler than a RCS's thrusters.

Some properties of this method are: 1) For an only spin-stabilized spacecraft, only the spin about the axis of maximum moment of inertia is stable. 2) In some spacecraft nutational or coning instability has been observed thus, for nutation control a RCS should be employed (see [6-8]). 3) Nutation may result in resonance in spacecraft flexible parts [9-11]. 4) Without an active control system (such as RCSs) spin-axis stabilization (with respect to the desired inertial direction), cannot be achieved ([12-15]).

RCSs are very useful to attenuate disturbances and perform attitude control. They have disadvantages and requirements which are: 1) they increase the complexity, mass and cost of a spacecraft. 2) Because of using liquid propellants in RCSs, fuel sloshing is presented; in this condition attitude control of spacecraft is very difficult. There are several researches ([16-19]) on the slosh dynamics and their control. In [16, 20-22] it is shown that many external torques are needed for control of the rocket engine with fuel sloshing. 3) since they are inherently nonlinear actuators, a complex control logic is needed to transform the attitude control command into the RCSs command [23]. Although a combination of a RCS and TVC is a good choice for large spacecraft and upper stage vehicles (see [1,16,24-26]), they are not suitable to be used in a small spacecraft.

TVC method is based on directing the thrust vector through the C.M of spacecraft. This powerful technique with extremely advantages can work with a servo actuator without fuel consumption. The active control torque generated by this method can easily overcome to the disturbance created by the thrust vector misalignment [27]. When the disturbance level is so larger than the attitude control capacity, a fixed thrust system is not efficient and applicable (Apollo, Cassini [28], [29] and launchers). gimbaled-TVC is more simpler than the other TVC methods such as moving plate (see [30]) which are accompanied by a highly nonlinear behavior. It is also used in a solar-sail spacecraft [31]. Recently, the company SpaceX is providing the terminal guidance and landing capability of Falcon-9 rocket with a new technology of TVC system. The gimbaled-thruster enable us to preserve weight, simplify attitude control system and reduce the requirements of the C.M positioning accuracy ([2], [3], [26]). In general, when the

Corresponding author, E-mail: kabgan@aut.ac.ir

liquid propellant rockets are used, the dynamical interaction between the movable nozzle and body is very small (see [1, 16, 20, 21]). But for a small spacecraft equipped with a solid rocket motor (SRM), the mentioned interaction makes a nonlinear two-body dynamics [3, 26].

Since momentum exchange devices (such as RWs and control moment gyro (CMG)) do not require any fuel consumption, they are very attractive for use in attitude control. They only transfer the momentum, but they cannot reject the external disturbance alone. Although a RW reaction torque is very smaller than the disturbance level, a large gyroscopic torque can be generated by the interaction between its angular momentum and the spacecraft spin rate.

In research [26] the nonlinear dynamics for an upper stage launcher equipped with a two-axis gimbaled-thruster is derived and a nonlinear control law based on a gimbal actuator and eight RCSs is designed. There was no challenge in control problem, because the mentioned system is over-actuated with several actuators. But the problem studied here is concerned with the control of an under-actuated spacecraft with only one control input.

In this paper in addition to the disturbance rejection, it is so desirable to align the thrust vector direction with the inertial z-direction (Z_I). In previous works these performances are achieved by using some thrusters (e.g., RCSs) which are not efficient for a small spacecraft. The goal of this paper is thrust vector stabilization and full disturbance rejection with a new structure of control system. The proposed structure includes a 1DoF gimbaled-thruster, two RWs and spin-stabilization. The goal is to show the advantages of this system in comparison with the other methods. In order to reject the exogenous disturbances, the RWs gyroscopic torques along with a least squares-based self-tuning controller (STC) is utilized. The object is to design a least squares-based estimator ([32, 33]) to guarantee the convergence of the estimated disturbances.

The remainder of the paper is organized as follows; in section 2 dynamics modeling is given. In section 3 the structure of the closed-loop control system is proposed including full state feedback controller for the gimbal actuator, feed-forward controller for RWs, and the least squares disturbance estimator. Finally, simulation results are drawn in section 4.

2- Dynamic Modeling

2- 1- Nonlinear dynamic modeling

In this section, the dynamics equation of the spacecraft (shown in Figure 1) is derived. It is assumed that the thruster (SRM) has a constant thrust of F_T.

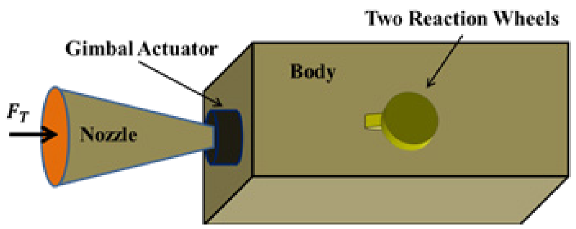

Fig. 1. A spin-stabilized spacecraft equipped with two RWs and a 1DoF gimbaled-thruster.

The free body diagram of the body and the nozzle are indicated in Figure 2. The nozzle (whole of the SRM) can rotate on axis x_s (x_n) using a 1DoF gimbal actuator at the pivot o. Subscripts s, n, o and T denote the body, the nozzle, gimbal pivot and the point of acting the thrust force, respectively. $x_sy_sz_s$ and $x_ny_nz_n$ are the body and the nozzle fixed frame respectively, which are placed in their C.Ms. G_s and G_n are the body and the nozzle C.M locations. $\tau_s \in R^3 (\tau_n)$ and $\omega_s \in R^3 (\omega_n)$ express the body (nozzle) external torque and the angular velocity, respectively. $M_0 \in R^3$ and $F_0 \in R^3$ are the interaction torques and forces at the pivot o, $\rho_{so} \in R^3$ is the vector from G_s to point o. $\rho_{no} \in R^3$ and $\rho_{nT} \in R^3$ are the relative vector from G_n to o and T, respectively. In Figure 3, β denotes the relative rotation of $x_ny_nz_n$ with respect to $x_sy_sz_s$.

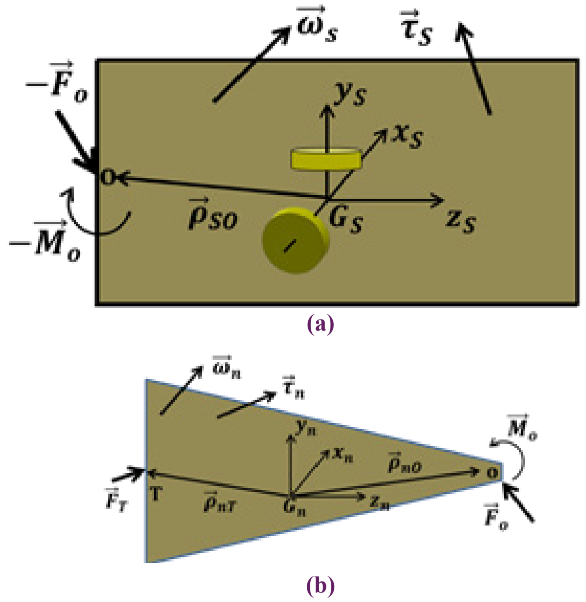

Fig. 2. Free body diagram of the body (a) and nozzle (b) with a 1DoF gimbal actuator at the pivot o and two RWs at the Gs.

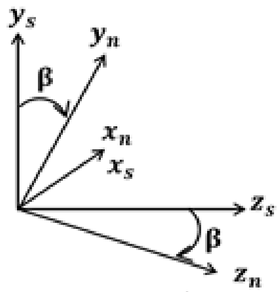

Fig. 3. Gimbal rotation β at the pivot o.

Euler momentum equations of the body and the nozzle are given in their coordinate frames as

$$\tau_s + \tau_{Rw} - \rho_{so} \times F_o - M_o = I_s \dot{\omega}_s + \omega_s \times (I_s \omega_s + \boldsymbol{H}_{Rw}), \quad (1)$$

$$\boldsymbol{\tau}_n^n + \boldsymbol{\rho}_{no}^n \times \boldsymbol{F}_o^n + \boldsymbol{M}_o^n + \boldsymbol{\rho}_{nT}^n \times \boldsymbol{F}_T^n = \boldsymbol{I}_n^n \dot{\boldsymbol{\omega}}_n^n + \boldsymbol{\omega}_n^n \times (\boldsymbol{I}_n^n \boldsymbol{\omega}_n^n), \quad (2)$$

where, the superscript s and n describe a vector in $x_sy_sz_s$ and $x_ny_nz_n$, respectively; for simplicity the superscript s is not shown. I_s and I^n_n are the moment of inertia of the body and the nozzle, respectively, $\boldsymbol{H}_{Rw} = \begin{bmatrix} h_{r,x} & h_{r,y} & 0 \end{bmatrix}^T$ and $\tau_{Rw} = \begin{bmatrix} \tau_{r,x} & \tau_{r,y} & 0 \end{bmatrix}^T$ denote the RWs angular momentum and axial torques,

where, $\dot{\boldsymbol{H}}_{Rw} = -\boldsymbol{\tau}_{Rw}$. (3)

The following rotation matrix is used to transform Eq.(2) to s frame

$$\boldsymbol{R}_n^s(\beta) = \begin{bmatrix} 1 & 0 & 0 \\ 0 & cos(\beta) & -\sin(\beta) \\ 0 & \sin(\beta) & \cos(\beta) \end{bmatrix}, \quad (4)$$

After multiplying both sides of Eq.(2) by $\boldsymbol{R}_n^s$ and using the transformations given in Eq.(5)

$$\begin{cases}\tau_n = \boldsymbol{R}_n^s \tau_n^n, \boldsymbol{M}_o = \boldsymbol{R}_n^s \boldsymbol{M}_o^n, \boldsymbol{I}_n = \boldsymbol{R}_n^s \boldsymbol{I}_n^n \boldsymbol{R}_n^{sT}, \\ \rho_{no} \times \boldsymbol{F}_o = \boldsymbol{R}_n^s(\rho_{no}^n \times \boldsymbol{F}_o^n),\ \rho_{no} = \boldsymbol{R}_n^s \rho_{no}^n, \boldsymbol{F}_o = \boldsymbol{R}_n^s \boldsymbol{F}_o^n, \\ \rho_{nT} \times \boldsymbol{F}_T = \boldsymbol{R}_n^s(\rho_{nT}^n \times \boldsymbol{F}_T^n),\ \rho_{nT} = \boldsymbol{R}_n^s \rho_{nT}^n,\ \boldsymbol{F}_T = \boldsymbol{R}_n^s \boldsymbol{F}_T^n.\end{cases} \tag{5}$$

Eq.(2) is reformed to Eq.(6) as

$$\tau_n + \rho_{no} \times \boldsymbol{F}_o + \boldsymbol{M}_o + \rho_{nT} \times \boldsymbol{F}_T = \boldsymbol{I}_n \dot{\omega}_n + \omega_n \times (\boldsymbol{I}_n \omega_n). \tag{6}$$

The summation of Eq.(6) and Eq.(1) yields

$$\begin{gathered}\boldsymbol{\tau}_{ns} + \boldsymbol{\tau}_{Rw} + \boldsymbol{\rho}_{ns} \times \boldsymbol{F}_o + \boldsymbol{\rho}_{nT} \times \boldsymbol{F}_T = \boldsymbol{I}_{ns} \dot{\boldsymbol{\omega}}_s + \\ \boldsymbol{I}_n(\dot{\boldsymbol{\omega}}_r + \boldsymbol{\omega}_s \times \boldsymbol{\omega}_r) + \boldsymbol{\omega}_s \times (\boldsymbol{I}_s \boldsymbol{\omega}_s + \boldsymbol{H}_{Rw}) + \boldsymbol{\omega}_n \times (\boldsymbol{I}_n \boldsymbol{\omega}_n),\end{gathered} \tag{7}$$

where,

$$\begin{gathered}\omega_n = \omega_s + \omega_r, \dot{\omega}_n = \dot{\omega}_s + \dot{\omega}_r + \omega_s \times \omega_r,\ \tau_{ns} = \tau_s + \tau_n, \\ \rho_{ns} = \rho_{no} - \rho_{so}, \rho_{sn} = -\rho_{ns}, \boldsymbol{I}_{ns} = \boldsymbol{I}_s + \boldsymbol{I}_n,\end{gathered} \tag{8}$$

$\boldsymbol{\omega}_r$ and $\dot{\boldsymbol{\omega}}_r$ are the relative angular velocity and acceleration of the nozzle with respect to the body, respectively,

$$\omega_r = \begin{bmatrix}\dot{\beta} & 0 & 0\end{bmatrix}^T, \dot{\omega}_r = \begin{bmatrix}\ddot{\beta} & 0 & 0\end{bmatrix}^T. \tag{9}$$

In Eq.(7) F_0 should be replaced with the other known variables thus, the Newton's law for the both body and nozzle along with their C.M accelerations are given

$$\begin{cases}\boldsymbol{F}_T + \boldsymbol{F}_o = m_n \boldsymbol{a}_{Gn} \\ -\boldsymbol{F}_o = m_s \boldsymbol{a}_{Gs}\end{cases}, \begin{cases}\boldsymbol{a}_o = \boldsymbol{a}_{Gn} + \dot{\boldsymbol{\omega}}_n \times \boldsymbol{\rho}_{no} + \boldsymbol{\omega}_n \times (\boldsymbol{\omega}_n \times \boldsymbol{\rho}_{no}) \\ \boldsymbol{a}_o = \boldsymbol{a}_{Gs} + \dot{\boldsymbol{\omega}}_s \times \boldsymbol{\rho}_{so} + \boldsymbol{\omega}_s \times (\boldsymbol{\omega}_s \times \boldsymbol{\rho}_{so})\end{cases}. \tag{10}$$

where, m_s and m_n denote the body and the nozzle mass, respectively. The solution of the above equations yields

$$\begin{gathered}\boldsymbol{F}_o = -\boldsymbol{F}_T(M/m_n) + M(\dot{\boldsymbol{\omega}}_s \times \boldsymbol{\rho}_{sn} - (\dot{\boldsymbol{\omega}}_r + \boldsymbol{\omega}_s \times \boldsymbol{\omega}_r) \times \boldsymbol{\rho}_{no} \\ + \boldsymbol{\omega}_s \times (\boldsymbol{\omega}_s \times \boldsymbol{\rho}_{so}) - \boldsymbol{\omega}_n \times (\boldsymbol{\omega}_n \times \boldsymbol{\rho}_{no})),\end{gathered} \tag{11}$$

where, $M = (m_n m_s)/(m_n + m_s)$ By substituting F_0 in Eq.(7), $\dot{\boldsymbol{\omega}}_s$ as the body angular acceleration will be

$$\dot{\boldsymbol{\omega}}_s = \left[\boldsymbol{I}_{ns,T}\right]^{-1} \boldsymbol{T}_s$$

where,

$$\begin{aligned}\boldsymbol{T}_s = {} & \boldsymbol{\tau}_{ns} + \boldsymbol{\tau}_{Rw} + \boldsymbol{\rho}_T \times \boldsymbol{F}_T - \boldsymbol{I}_r(\dot{\boldsymbol{\omega}}_r + \boldsymbol{\omega}_s \times \boldsymbol{\omega}_r) \\ & + M\boldsymbol{\rho}_{ns} \times (\boldsymbol{\omega}_s \times (\boldsymbol{\omega}_s \times \boldsymbol{\rho}_{so}) - \boldsymbol{\omega}_n \times (\boldsymbol{\omega}_n \times \boldsymbol{\rho}_{no})) \\ & - \boldsymbol{\omega}_s \times (\boldsymbol{I}_s \boldsymbol{\omega}_s + \boldsymbol{H}_{Rw}) - \boldsymbol{\omega}_n \times (\boldsymbol{I}_n \boldsymbol{\omega}_n),\end{aligned}$$

$$\boldsymbol{T}_s = \begin{bmatrix}T_x & T_y & T_z\end{bmatrix}^T \qquad \boldsymbol{\omega}_s = \begin{bmatrix}\omega_{sx} & \omega_{sy} & \omega_{sz}\end{bmatrix}^T$$

$$\boldsymbol{I}_{ns,T} = \boldsymbol{I}_{ns} - M[\boldsymbol{\rho}_{ns}\times]^2,\ \boldsymbol{I}_r = \boldsymbol{I}_n - M[\boldsymbol{\rho}_{ns}\times][\boldsymbol{\rho}_{no}\times],$$

$$\boldsymbol{\rho}_T = \boldsymbol{\rho}_{nT} + \boldsymbol{\rho}_{sn}(M/m_n)$$

For a vector $\boldsymbol{s} = [s_1 \quad s_2 \quad s_3]^T$, the operator $[\boldsymbol{s}\times]$ is defined by

$$[\boldsymbol{s}\times] = \begin{bmatrix}0 & -s_3 & s_2 \\ s_3 & 0 & -s_1 \\ -s_2 & s_1 & 0\end{bmatrix}.$$

2- 2- Spacecraft kinematics

The results of this section enable us to calculate the velocity increment vector Δv and thrust vector deviation from the inertial frame. The time derivative of the Euler angles that give the body attitude with respect to the inertial coordinate $X_I Y_I Z_I$ is obtained as

$$\begin{bmatrix}\dot{\varphi} & \dot{\theta} & \dot{\psi}\end{bmatrix}^T = \boldsymbol{J}_\omega^{Eu}(\varphi, \theta, \psi)\boldsymbol{\omega}_s, \tag{12}$$

where

$$\boldsymbol{J}_\omega^{Eu} = \begin{bmatrix}1 & \sin(\varphi)\tan(\theta) & \cos(\varphi)\tan(\theta) \\ 0 & \cos(\varphi) & -\sin(\varphi) \\ 0 & \sin(\varphi)/\cos(\theta) & \cos(\varphi)/\cos(\theta)\end{bmatrix}.$$

A desired velocity change Δv_d and burning time T_b define an orbital transfer mission. The actual velocity change Δv_z along the Z_I is achieved as

$$\Delta v_z = \int_0^{T_b} a_{\max}\cos(\delta_{FT}(t))dt, \tag{13}$$

where, $\delta_{FT}(t) = \cos^{-1}\left(\cos(\theta(t))\cos(\varphi(t) + \beta(t))\right)$ is the thrust vector deviation from Z_I and a_{max} is obtained as

$$a_{\max} = \Delta v_d / T_b,\ F_T = a_{\max}(m_s + m_n). \tag{14}$$

Since $\delta_{FT}(t)$ is always nonzero in practice, and then $\Delta v_z < \Delta v_d$ can be easily concluded.

2- 3- Linearization of the nonlinear model

In this section, based on some assumptions, the nonlinear model ((11) and (12)) will be linearized. Some assumptions on the parameters are chosen as

$$\begin{gathered}\boldsymbol{F}_T^n = \begin{bmatrix}0 & 0 & F_T\end{bmatrix}^T, \boldsymbol{\rho}_{no}^n = \begin{bmatrix}0 & 0 & z_n\end{bmatrix}^T, \boldsymbol{\rho}_{nT}^n = \boldsymbol{0}_{3\times1}, \\ \boldsymbol{\rho}_{so} = \begin{bmatrix}x_s & y_s & -z_s\end{bmatrix}^T, \boldsymbol{I}_n^n = \mathrm{diag}(I_{n2}, I_{n2}, I_{n1}), \\ \boldsymbol{I}_s = \mathrm{diag}(I_{s2}, I_{s2}, I_{s1}), \boldsymbol{\omega}_s(0) = \begin{bmatrix}0 & 0 & \bar{\omega}_s\end{bmatrix}^T.\end{gathered} \tag{15}$$

where, z_s and z_n denote the distance of the pivot from the C.Ms of the body and the nozzle. x_s and y_s denote the C.M offsets of the body, respectively. I_{s2} and I_{n2} are the transverse moments of inertia of the body and nozzle, respectively. I_{s1} and I_{n1} denote the moment of inertia about the axes z_s and z_n. $\bar{\omega}_s$ is the initial spin-rate about the spacecraft longitudinal axis. As noticed earlier the disturbance generated by thrust vector misalignments is the most important input to the spacecraft dynamics. in this work such as [22] and [26], disturbances are assumed to be constant (a constant C.M offset). From the dynamics (11), the disturbance created by the C.M offsets x_s and y_s will be

$$\bar{\tau}_{dx} = (F_T M y_s)/m_n,\ \bar{\tau}_{dy} = -(F_T M x_s)/m_n, \tag{16}$$

Usually for a spin-stabilized spacecraft the angular momentum about the longitudinal axis (due to spin-rate) is enough large for which the spin rate can be considered nearly constant or having

$$\dot{\omega}_{sz}(t) \approx 0 \Rightarrow \omega_{sz} \approx \bar{\omega}_s.$$

Since the control object is not to stabilize the spacecraft revolute rotation; therefor, angle Ψ can be an arbitrary value with $\dot{\psi} \approx \omega_{sz} \approx \bar{\omega}_s$ The state vector that should be controlled is $\boldsymbol{X} = [\varphi \quad \theta \quad \omega_{sx} \quad \omega_{sy} \quad \beta \quad \dot{\beta}]^T$.

Now by considering a small variation for the partial states (X) and using Eqs. (15) and (16), the state space model is obtained here

$$\dot{\boldsymbol{X}}(t) = \boldsymbol{A}\boldsymbol{X}(t) + \boldsymbol{B}u(t) + \bar{\boldsymbol{D}}(t), \tag{17}$$

where,

$$A=\begin{bmatrix} 0 & \bar{\omega}_s & 1 & 0 & 0 & 0 \\ -\bar{\omega}_s & 0 & 0 & 1 & 0 & 0 \\ 0 & 0 & 0 & -\lambda & -I_\beta & 0 \\ 0 & 0 & \lambda & 0 & 0 & I_{nM}\bar{\omega}_s \\ 0 & 0 & 0 & 0 & 0 & 1 \\ 0 & 0 & 0 & 0 & 0 & 0 \end{bmatrix},$$

$$B=\begin{bmatrix} 0 \\ 0 \\ -I_r \\ 0 \\ 0 \\ 1 \end{bmatrix}, \bar{D}(t)=\begin{bmatrix} 0 \\ 0 \\ \bar{\tau}_{dx}+\tau_{rx}(t)+\bar{\omega}_s h_{ry}(t) \\ \bar{\tau}_{dy}+\tau_{ry}(t)-\bar{\omega}_s h_{rx}(t) \\ 0 \\ 0 \end{bmatrix}(\frac{1}{I_2})$$

, and

$I_1=I_{n1}+I_{s1}, I_2=I_{n2}+I_{s2}+M(z_n+z_s)^2, (I_1-I_2)\bar{\omega}_s=I_2\lambda,$

$I_{n2}+M(z_n+z_s)z_n=I_r I_2, I_{n1}-I_{n2}-M(z_n+z_s)z_n=I_{nz}I_2,$

$(F_T M z_s)/m_n+I_{nz}I_2\bar{\omega}_s^2=I_\beta I_2,$

$I_{nm}=I_{nz}-I_r \Leftrightarrow (I_{n1}-2I_{n2}-2M(z_n+z_s)z_n)=I_{nm}I_2,$

$\ddot{\beta}=u$ is the control input and $\bar{D}(t)$ includes the constant disturbances, the RWs axial torques as well as their gyroscopic torques ($\bar{\omega}_s h_{ry}(t)$ and $\bar{\omega}_s h_{rx}(t)$).

3- Closed-Loop Control System Design

In this section, at first a full state feedback controller based on control input u is introduced to stabilize the partial states X and then based on the two RWs, a feed-forward controller is designed to reject the disturbances in two axes. Next the least squares estimator is formulated to estimate the disturbances.

3- 1- TVC based full state feedback controller

When the disturbances are not presented, a full state feedback controller must be able to stabilize the following system

$$\dot{X}(t)=AX(t)+Bu(t).$$

Then the following controller can guarantee the stability of the above system if the pair (A, B) be controllable

$$u(t)=-KX(t),\ K\in R^{1\times n} \tag{18}$$

By using a proper gain K, $\tilde{A}=A-BK$ will be stable. Then, for a positive symmetric matrix $Q>0$ there is a unique positive symmetric matrix P such that Lyapunov equation is satisfied in Eq.(19).

$$\tilde{A}^T P+P\tilde{A}=-Q \tag{19}$$

Since the system is single-input, Co must be full rank. As can be seen, generally $|Co|\neq 0$ is concluded.

$$Co=\left[B, AB, A^2B, A^3B, A^4B, A^5B\right]$$

$$\Rightarrow |Co|=\lambda\bar{\omega}_s(\lambda-\bar{\omega}_s)^2(\mathrm{F_T M}z_s/(m_n I_2))^2(-I_r\lambda^2+I_{nm}\bar{\omega}_s\lambda+I_\beta)^2.$$

The conditions by which (A, B) is not controllable are:

1) $\bar{\omega}_s=0$, 2) $\lambda=0\ (I_1=I_2)$,

3) $\lambda=\bar{\omega}_s\ (I_1=2I_2)$, 4) $-I_r\lambda^2+I_{nM}\omega_s\lambda+I_\beta=0$

3- 2- RW based feed-forward controller

At what follows, we show that the RWs gyroscopic torques is able to reject the constant disturbances $\bar{\tau}_{dx}$ and $\bar{\tau}_{dy}$. At first under the stabilizing control law (18), the closed-loop system will be

$$\dot{X}(t)=\tilde{A}X(t)+\bar{D}(t). \tag{20}$$

Consider the following Lyapunov function candidate

$$V(t)=X^T(t)PX(t).$$

The time derivative of V(t) along Eq.(19) and Eq.(17) will be

$$\begin{aligned} \dot{V}&=X^T(t)\left[\tilde{A}^T P+P\tilde{A}\right]X(t)+2X^T(t)PD(t) \\ &=-X^T(t)QX(t)+2X^T(t)PD(t) \end{aligned} \tag{21}$$

It can be easily concluded that

$$\textit{if}\ \ D(t)\to 0 \Rightarrow \dot{V}<0 \Rightarrow X(t)\to 0\ \ as\ \ t\to\infty.$$

We show that by using the RWs gyroscopic torque the two terms of $\bar{D}_3(t)=\bar{\tau}_{dx}+\tau_{rx}(t)+\bar{\omega}_s h_{ry}(t)$ and $\bar{D}_4(t)=\bar{\tau}_{dy}+\tau_{ry}(t)-\bar{\omega}_s h_{rx}(t)$ converge to zero. By employing the control law

$$\tau_{rx}=\tau_{Rm}\tanh(\gamma e_{rx}),\quad \tau_{ry}=\tau_{Rm}\tanh(\gamma e_{ry}), \tag{22}$$

$\bar{D}_3(t)\to 0$ and $\bar{D}_4(t)\to 0$ as $t\to\infty$ will be concluded where, τ_{Rm} denotes maximum reaction torque of the RWs, $e_{rx}(t)=h_{rx}(t)-\bar{\tau}_{dy}/\bar{\omega}_s$ and $e_{ry}(t)=h_{ry}(t)+\bar{\tau}_{dx}/\bar{\omega}_s$ are the angular momentum tracking errors and γ is the positive gain. By defining the Lyapunov functions $V_{ex}=e_{rx}^2/2$ and $V_{ey}=e_{ry}^2/2$, and using Eq.(3), the convergence of the $\bar{D}_3(t)$ and $\bar{D}_4(t)$ can be easily concluded.

3- 3- Least squares based disturbance estimator

In this section, a least squares based STC ([34]-Ch8) is designed to estimate the disturbances then the estimated disturbances are fed-forward to the RWs controller. We use the least squares method with a constant forgetting factor. This estimate potentially has the advantage of averaging out the effects of measurement noises.

Since the disturbance $\bar{\tau}_{dx}$ and $\bar{\tau}_{dy}$ (dut to x_s and y_s) are unknown we reformed Eq.(11) to

$$I_{ns,T}\dot{\omega}_s \approx T_{s,0}+\left[\bar{\tau}_{dx}\quad \bar{\tau}_{dy}\quad 0\right]^T, \tag{23}$$

where, $T_{s,0}=T_s\big|_{x_s=y_s=0}$ is calculated with $x_s=y_s=0$. Then we multiply both sides of Eq.(23) by C to obtain the following form

$$C(I_{ns,T}\dot{\omega}_s-T_{s,0})=a \tag{24}$$

where, $C=\begin{bmatrix}1 & 0 & 0\\ 0 & 1 & 0\end{bmatrix}$, and vector $a=\left[\bar{\tau}_{dx}\quad \bar{\tau}_{dy}\right]^T$ contains unknown parameters to be estimated.

The above model cannot be directly used for estimation, because $\dot{\omega}_s$ appears in the above equation (note that numerically differentiating ω_s is usually undesirable because of noise considerations).

To eliminate $\dot{\omega}_s$ in the above equation, let us filter (multiply) both sides of the above equation by $\eta/(s+\eta)$ (the impulse response is $f(t)=\eta\exp(-\eta(t))$). Then, convolving both sides of Eq.(24) by $f(t)$ yields

$$Y_f(t)=C\int_0^t f(t-r)(I_{ns,T}(r)\dot{\omega}_s(r)-T_{s,0}(r))dr=\int_0^t f(t-r)dr\,a$$

Using partial integration, the above equation can be rewritten as linear parametrization form

$$Y_f(t)=W_f(t)a\ \ \text{with}\ \ Y_f(t)=y_1+y_2+y_3 \tag{25}$$

where,

$$y_1=C\left(\eta I_{ns,T}(t)\omega_s(t)-f(t)I_{ns,T}(0)\omega_s(0)\right),$$

$$y_2=-C\int_0^t f(t-r)\left(\eta I_{ns,T}(r)+\dot{I}_{ns,T}(r)\right)\omega_s(r)dr,$$

$$y_3=-C\int_0^t f(t-r)T_{s,0}(r)dr,$$

and $W_f = (1-\exp(-\eta t))$ is the signal matrix.

Now we can use the following standard formulas for parameter update law,

$$\dot{\Gamma} = \sigma\Gamma - \Gamma W_f^T W_f \Gamma \Rightarrow \dot{\Gamma} = \sigma\Gamma - \Gamma^2 W_f^2(t),$$

$$\boldsymbol{e}_t = \hat{\boldsymbol{Y}}_f(t) - \boldsymbol{Y}_f(t) = W_f(t)\hat{\boldsymbol{a}} - \boldsymbol{Y}_f(t),$$

$$\dot{\hat{\boldsymbol{a}}} = -\Gamma W_f(t)\boldsymbol{e}_t,$$

where, Γ is the estimator gain matrix, σ is constant forgetting factor and e_t is tracking error. $\Gamma(0)$ can be chosen to be diagonal, for simplicity. Since W_f is scalar therefore, according to above equation $\Gamma(t)$ will be always diagonal as

$$\boldsymbol{\Gamma}(t) = \begin{bmatrix} \gamma_x(t) & 0 \\ 0 & \gamma_y(t) \end{bmatrix} \text{ and } \boldsymbol{\Gamma}^2(t) = \begin{bmatrix} \gamma_x^2(t) & 0 \\ 0 & \gamma_y^2(t) \end{bmatrix}.$$

At the following we show that for a constant forgetting factor σ, $\gamma_x \to \sigma$ as $t \to \infty$ and $\gamma_x(t) > 0$ for each $\gamma_x(0) > 0$.

The gain update law for γ_x is

$$\dot{\gamma}_x = \sigma\gamma_x - \gamma_x^2(1-\exp(-\eta t))^2.$$

At first it is rewritten as

$$\frac{d(\gamma_x^{-1})}{dt} = -\sigma\gamma_x^{-1} + (1-\exp(-\eta t))^2.$$

The solution of the above ode is

$$\gamma_x^{-1}(t) = \exp(-\sigma t)\gamma_x^{-1}(0) + \int_0^t \exp(-\sigma(t-r))(1-\exp(-\eta r))^2 dr$$

$$= \exp(-\sigma t)\gamma_x^{-1}(0) + \left(\frac{1}{\sigma} - 2\frac{\exp(-\eta t)}{\sigma-\eta} + \frac{\exp(-2\eta t)}{\sigma-2\eta}\right)$$

$$-\exp(-\sigma t)\left(\frac{1}{\sigma} - \frac{2}{\sigma-\eta} + \frac{1}{\sigma-2\eta}\right).$$

It is easy to see that $\gamma_x \to \sigma$ as $t \to \infty$. The mentioned result can be also achieved for $\gamma_y(t)$, similarly.

The convergence of the estimated disturbances to the true disturbances depends on the excitation of the signals. The following lemma ([34]-Ch8), guarantees the parameters error convergence

$$\lambda_{\min}\left(\int_0^t W^T W dr\right) = \int_0^t W_f^2(r)dr = \int_0^t (1-\exp(-\eta t))^2 dr \to \infty \quad as \quad t \to \infty$$

where, $\gamma_{\min}(.)$ denotes the smallest eigenvalue, then the, estimated disturbances asymptotically converge to the actual values.

4- Numerical Simulations

In this section, to show the applicability of the proposed method as well as its controller ability, a numerical simulation is carried out. The spacecraft and controller parameters are given at the following.

$\Delta v_d = 100\,m/s$, $T_b = 50s$, $\tau_{Rm} = 0.1$Nm, $\gamma = 10$, $\bar{\tau}_{dx} = 4$Nm,
$\bar{\tau}_{dy} = 6$Nm, $I_{s2} = 10kgm^2$, $I_{s1} = 2.4I_{s2}$, $I_{n2} = 1kgm^2$, $I_{n1} = 0.5I_{n2}$,
$m_s = 150kg$, $m_s = 8kg$, $z_n = 0.2m$, $z_s = 0.75m$, $\bar{\omega}_s = 3.5rad/s$.
$\sigma = 2$, $\eta = 0.5$, $\boldsymbol{K} = [10.73, -42.24, -16.66, 1.15, 80.06, 10.98]$

The maximum acceleration and thrust force will be a_{max}=2m/s^2 and F_T=(m_n+m_s) a_{max}=316N, respectively. $\bar{\tau}_{dx}$ and $\bar{\tau}_{dy}$ are equivalent to C.M offsets of y_s=1.32cm and x_s=2cm, respectively. Assume that X(0)=0 to emphasize the disturbance effect on the performances. Note that the nonlinear plant is used but with the linear controller. In Figure 4 the Simmechanics model of spacecraft is presented by which the mathematical model will be validated. In addition to the other properties, $\delta_{FT,m}$ and $\bar{\delta}_{FT}$ are also studied where, they stand for the maximum and mean values of thrust vector devotion, respectively.

Spacecraft body attitude(φ,θ) and thrust vector deviation (δ_{FT}) are shown in Figure 5. It is seen that δ_{FT} is fully eliminated with the maximum overshoot of $\delta_{FT,m}$=7.12^0 and the average value of $\bar{\delta}_{FT} = 1.27^0$ .By passing the time the spin-axis stabilization is performed while the disturbances are fully rejected by the gyroscopic effect of the RWs. The transverse angular velocity (ω_{sx} and ω_{sy}) stabilization and the velocity change components (v_x, v_y and v_z) are drawn in Figure 6. An accurate velocity change v_z=99.90m/s is achieved in comparison with Δv_d=100m/s, that shows the effectiveness of the proposed method. The gimbal angle β, its rate $\dot{\beta}$ and control input, $u = \ddot{\beta}$ are shown in Figure 7. The maximum deflection of gimbal angle is -2.5deg. As can be seen in Figure 8 the RWs are activated by their maximum reaction torques (τ_{Rm}=0.1Nm) to reject the disturbances fast. The maximum axial torque of the RWs (τ_{Rm}=0.1Nm) is so smaller than the disturbance torques level, but their gyroscopic torques ($\bar{\omega}_s h_{rx} = 3.5\times1.71 \approx 6Nm$ and $-\bar{\omega}_s h_{ry} = 3.5\times1.14 \approx 4Nm$) can easily reject the disturbances. Least squares estimation errors and estimated disturbances are given in Figure 9 where the disturbances are completely estimated in less than 5s. In Figure 10 the histories of spin rate ω_{sz} and its small variation is drawn.

In Figure 11 and Figure 12 the DCM (directional cosine matrix) error, error of angular and linear velocity between the Simmechanics and dynamics model are given. These results validate the accuracy of the spacecraft dynamics mathematical modeling.

The important observations of this section are:

1. Disturbance rejection along with spin-axis and thrust vector stabilization is performed without attitude control systems that need to propellant (such as RCSs); RCSs are able to reject the disturbances, but the propellant is being consumed until the end of burning.
2. Regarding to the small RWs axial torques, the gyroscopic torque originated by the interaction between the RWs angular momentum and spin rate, can easily reject the exogenous disturbance.
3. For an only spin-stabilized spacecraft or a spacecraft with only gimbaled-TVC, thrust vector stabilization is not possible in presence of exogenous disturbances.
4. A RW is a momentum exchange device, in order to reject the external disturbance torques, the TVC must be also employed.
5. In the proposed method the velocity increments are enough accurate for an impulsive orbital maneuver.
6. The proposed method can stabilize the initial attitude (due to an undesired orientation) while rejecting the exogenous disturbance.
7. Least-squares based self-tuning controller can be implemented by which fast disturbance estimation can be achieved.

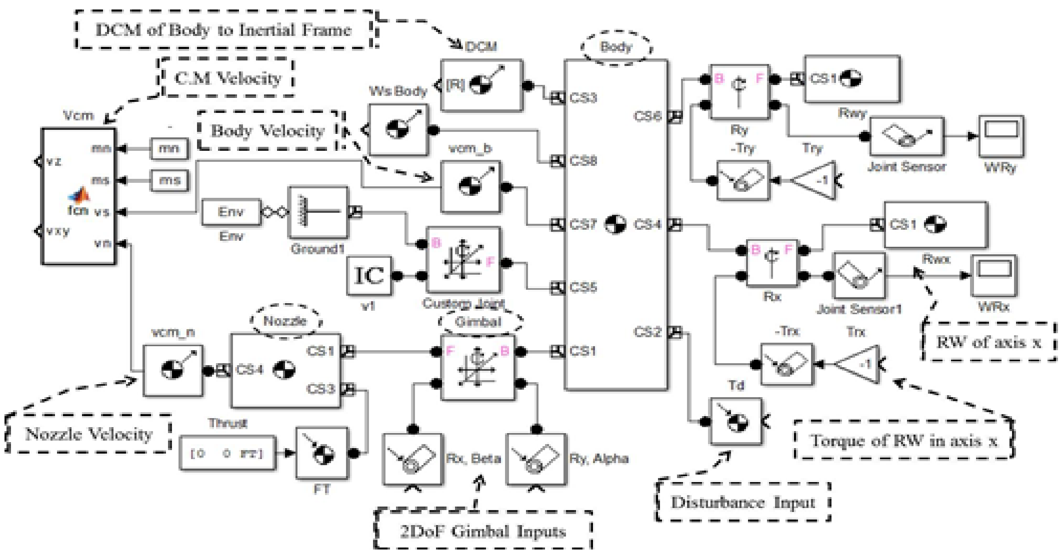

Fig. 4. Simmechanics model of the nonlinear plant with a 2DoF gimbal actuator and two RWs

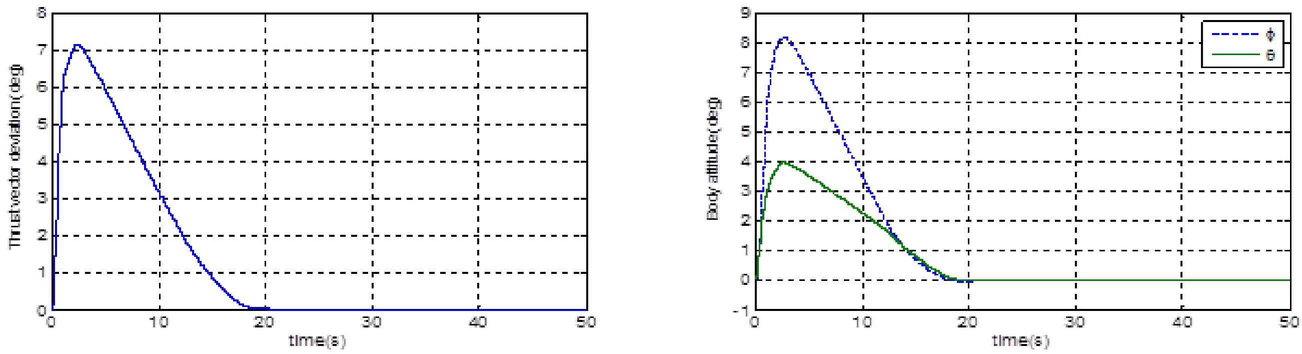

Fig. 5.Attitude (φ,θ) and thrust vector deviation (δ_{FT})

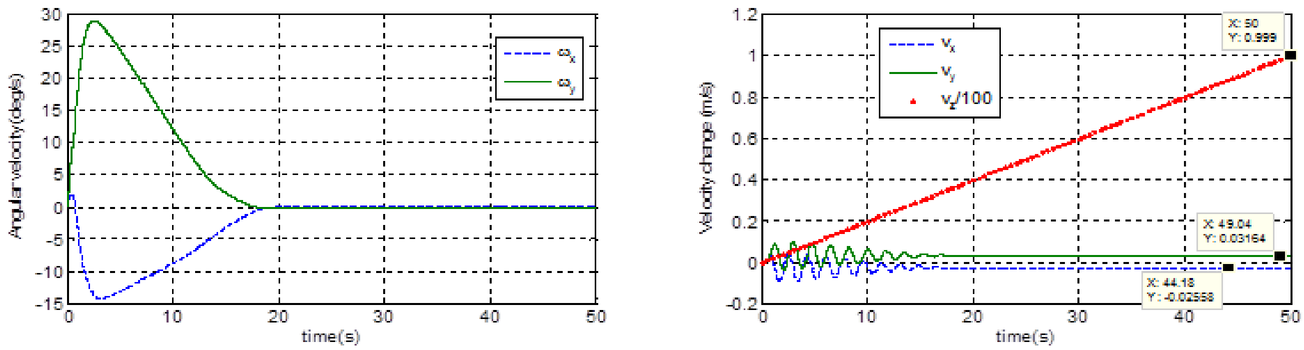

Fig. 6. The body angular velocity (ω_{sx} and ω_{sy}) and velocity change components (Δv).

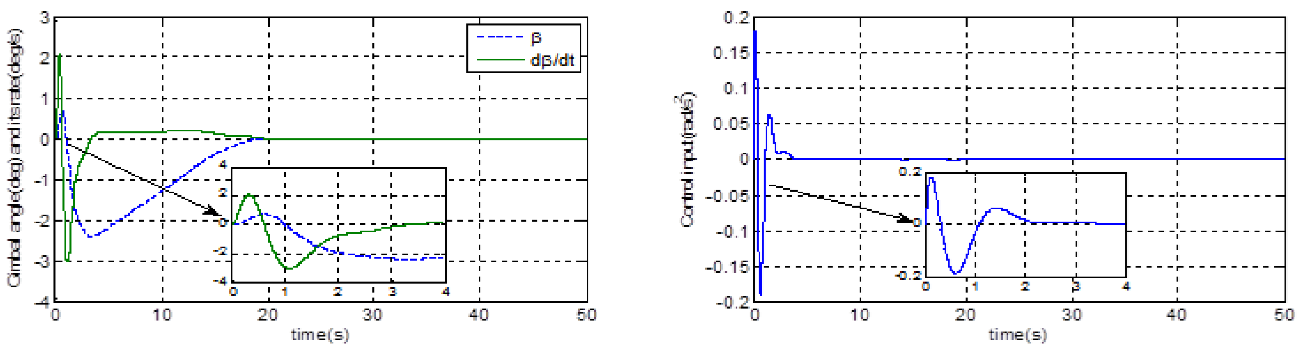

Fig. 7. Gimbal angle and its rate (β, $\dot{\beta}$), and control input u

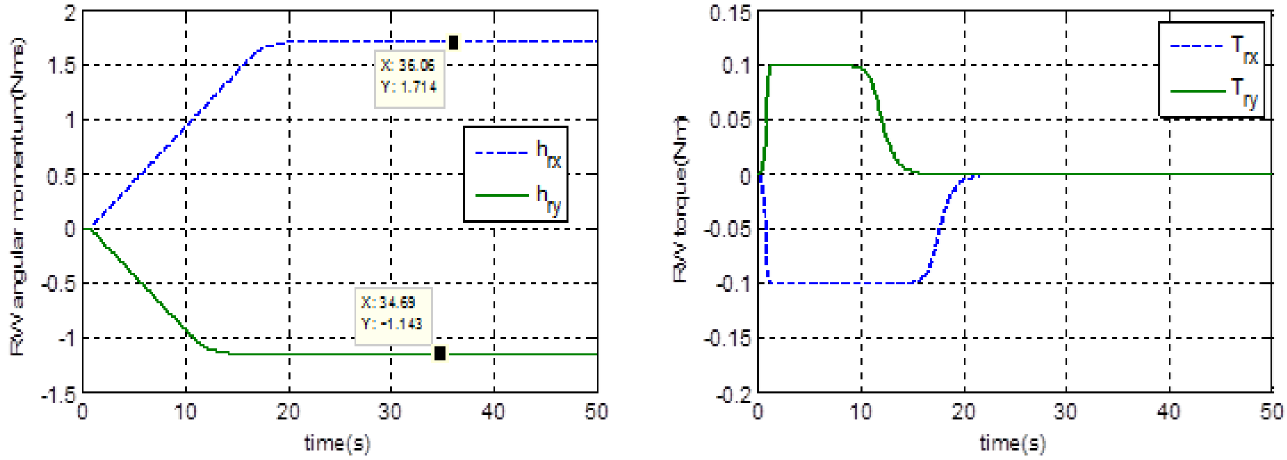

Fig. 8. The RWs angular momentum and their axial reaction torques

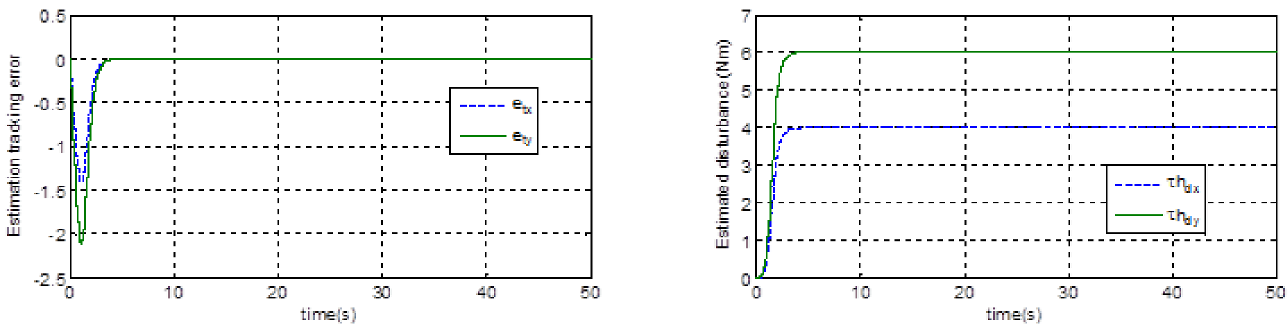

Fig. 9. Least squares estimation errors and estimated disturbances

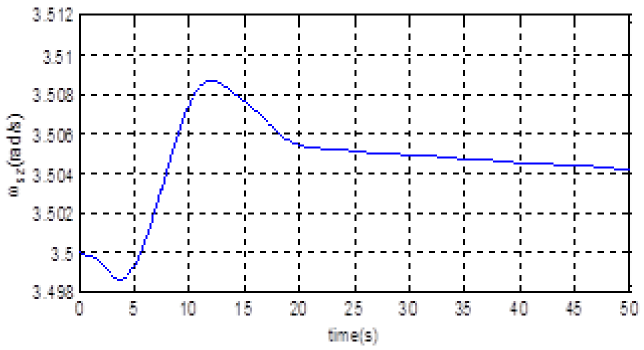

Fig. 10. Actual spin rate of spacecraft (ω_{sz})

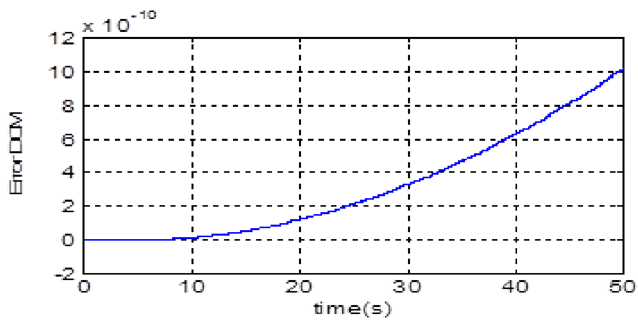

Fig. 11. DCM error between Simmechanics and dynamics model

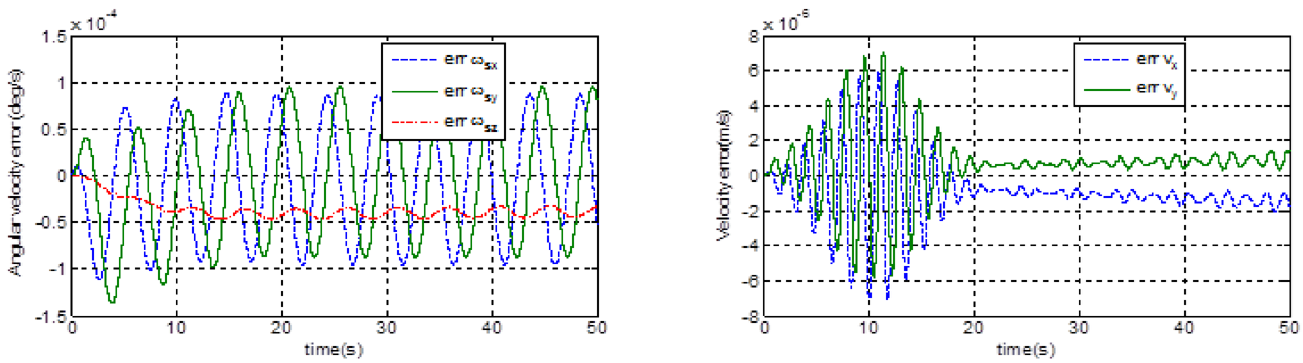

Fig. 12. Error of angular and linear velocity between the Simmechanics and dynamics model

5- Conclusion

According to the advantages of the gimbaled-TVC, RWs and spin-stabilization, a new thrusting maneuver system is introduced where the attitude stabilization and disturbance rejection are achieved without RCSs. Using the interaction of the RWs angular momentum (as the momentum exchange devices) and spin-rate, a new mechanism is designed for rejecting of external disturbances. It is shown that the underactuated spacecraft with only one active control part is controllable. For disturbance rejection, a feed-forward control law is proposed based on the RWs gyroscopic torque where the RWs are activated by their maximum axial torques. Simulation results show that in spite of exogenous disturbances caused by the C.M offsets, all state variables converge to zero. Disturbances are fully rejected in the proposed method. Using the least squares based self-tuning controller the disturbances are estimated in less than 5s (burning time is 50s). The results show the usefulness of the proposed method in practice. The proposed method can be a good choice for space vehicles with long term missions as well as to use in upper stage vehicles.

References

[1] J.S. Orr, Y.B. Shtessel, Lunar spacecraft powered descent control using higher-order sliding mode techniques, Journal of the Franklin Institute, 349(2) (2012) 476-492.

[2] R. Noll, Spacecraft Attitude Control During Thrusting Maneuvers, NASA SP-8059, (1971).

[3] H. Kouhi, M. Kabganian, M. Shahravi, F. Fani Saberi, Retrofiring control method via combination of a 1DoF gimbaled thrust vector control and spin-stabilization, Proceedings of the Institution of Mechanical Engineers, Part G: Journal of Aerospace Engineering, (2016).

[4] J.A. Oldenburg, S.G. Tragesser, Minimizing the effects of transverse torques during thrusting for spin-stabilized spacecraft, Journal of Guidance, Control, and Dynamics, 25(3) (2002) 591-595.

[5] J.K. Thienel, F.L. Markley, Comparison of Angular Velocity Estimation Methods for Spinning Spacecraft, in: Advances in Astronautical Science," AAS/AIAA Guidance, Navigation, and Control Conference, 2011.

[6] R. Meyer, Coning instability of spacecraft during periods of thrust, Journal of spacecraft and rockets, 33(6) (1996) 781-788.

[7] F.L. Janssens, J.C. Van Der Ha, Stability of spinning satellite under axial thrust and internal mass motion, Acta Astronautica, 94(1) (2014) 502-514.

[8] K.M. Martin, J.M. Longuski, Velocity Pointing Error Reduction for Spinning, Thrusting Spacecraft via Heuristic Thrust Profiles, Journal of spacecraft and rockets, 52(4) (2015) 1268-1272.

[9] G. Cloutier, Resonances of a two-DOF system on a spin-stabilized spacecraft, AIAA Journal, 14(1) (1976) 107-109.

[10] P. Meehan, S. Asokanthan, Control of chaotic motion in a spinning spacecraft with a circumferential nutational damper, Nonlinear Dynamics, 17(3) (1998) 269-284.

[11] G.J. Cloutier, Nutation damper instability on spin-stabilized spacecraft, AIAA Journal, 7(11) (1969) 2110-2115.

[12] P. Tsiotras, J.M. Longuski, Spin-axis stabilization of symmetric spacecraft with two control torques, Systems & Control Letters, 23(6) (1994) 395-402.

[13] [13] D.W. Childs, Fuel-optimal direction-cosine attitude control for spin-stabilized axisymmetric spacecraft, Journal of spacecraft and rockets, 7(12) (1970) 1481-1483.

[14] D.W. Childs, B.D. Tapley, W.T. Fowler, Suboptimal attitude control of a spin-stabilized axisymmetric spacecraft, Automatic Control, IEEE Transactions on, 14(6) (1969) 736-740.

[15] H. Gui, G. Vukovich, Robust adaptive spin-axis stabilization of a symmetric spacecraft using two bounded torques, Advances in Space Research, 56(11) (2015) 2495-2507.

[16] M. Reyhanoglu, J.R. Hervas, Nonlinear dynamics and control of space vehicles with multiple fuel slosh modes, Control Engineering Practice, 20(9) (2012) 912-918.

[17] B. Bandyopadhyay, P. Gandhi, S. Kurode, Sliding mode observer based sliding mode controller for slosh-free motion through PID scheme, Industrial Electronics, IEEE Transactions on, 56(9) (2009) 3432-3442.

[18] L.D. Peterson, E.F. Crawley, R.J. Hansman, Nonlinear fluid slosh coupled to the dynamics of a spacecraft, AIAA Journal, 27(9) (1989) 1230-1240.

[19] A. Shekhawat, C. Nichkawde, N. Ananthkrishnan, Modeling and stability analysis of coupled slosh-vehicle dynamics in planar atmospheric flight, in: Proc. 44th AIAA Aerospace Sciences Meeting and Exhibit, Reno, Nevada, 2006, pp. 2006-2427.

[20] J.R. Hervas, M. Reyhanoglu, Thrust-vector control of a three-axis stabilized upper-stage rocket with fuel slosh dynamics, Acta Astronautica, 98 (2014) 120-127.

[21] J. Rubio Hervas, M. Reyhanoglu, Thrust-vector control of a three-axis stabilized upper-stage rocket with fuel slosh dynamics, Acta Astronautica, 98 (2014) 120-127.

[22] W.A. Kishore, S. Dasgupta, G. Ray, S. Sen, Control allocation for an over-actuated Satellite Launch Vehicle, Aerospace Science and Technology, 28(1) (2013) 56-71.

[23] R.A. Hall, S. Hough, C. Orphee, K. Clements, Design and Stability of an On-Orbit Attitude Control System Using Reaction Control Thrusters, in: AIAA Guidance, Navigation, and Control Conference, 2016, pp. 0087.

[24] F.-K. Yeh, Sliding-mode-based contour-following controller for guidance and autopilot systems of launch vehicles, Proceedings of the Institution of Mechanical Engineers, Part G: Journal of Aerospace Engineering, 227(2) (2013) 285-302.

[25] W.S. Widnall, The minimum-time thrust-vector control law in the Apollo lunar-module autopilot, Automatica, 6(5) (1970) 661-672.

[26] Z. Wang, Y. Jia, L. Jin, J. Duan, Thrust Vector Control of Upper Stage with a Gimbaled Thruster during Orbit Transfer, Acta Astronautica, (2016).

[27] L. Felicetti, M. Sabatini, A. Pisculli, P. Gasbarri, G.B. Palmerini, Adaptive Thrust Vector Control during On-Orbit Servicing, in: Proceedings of AIAA SPACE 2014 Conference and Exposition, paper AIAA-2014-4341, San Diego, 2014.

[28] F. Rizvi, R.M. Weitl, Characterizing Limit Cycles in the

Cassini Thrust Vector Control System, Journal of Guidance, Control, and Dynamics, 36(5) (2013) 1490-1500.

[29] J.M.a.B. Reed, Implementation of the Orbital Maneuvering System Engine and Thrust Vector Control for the European Service Module, (2014).

[30] F. Kong, Y. Jin, H.D. Kim, Thrust vector control of supersonic nozzle flow using a moving plate, Journal of Mechanical Science and Technology, 30(3) (2016) 1209-1216.

[31] E. Sperber, B. Fu, F. Eke, Large Angle Reorientation of a Solar Sail Using Gimballed Mass Control, The Journal of the Astronautical Sciences, (2016) 1-21.

[32] M. Bayani, R. Kazemi, S. Azadiiii, Vehicle stabilization via a self-tuning optimal controller, Amirkabir International Journal of Modeling, Identification, Simulation & Control, 43(2) (2011) 33-41.

[33] H. Milanchian, J. Keighobadi, H. Nourmohammadi, Magnetic Calibration of Three-Axis Strapdown Magnetometers for Applications in Mems Attitude-Heading Reference Systems, Amirkabir International Journal of Modeling, Identification, Simulation & Control, 47(1) (2015) 55-65.

[34] J.-J.E. Slotine, W. Li, Applied nonlinear control, prentice-Hall Englewood Cliffs, NJ, 1991.

Please cite this article using:

H. Kouhi, M. Kabganian, F. Fani Saberi, M. Shahravi,"Adaptive Control of a Spin-Stabilized Spacecraft Using two Reaction Wheels and a 1DoF Gimbaled-Thruster", *AUT J. Model. Simul.*, 49(1)(2017)103-112.

DOI: 10.22060/miscj.2016.834